Measurement 221 (2023) 113524

Contents lists available at ScienceDirect

Measurement

journal homepage: www.elsevier.com/locate/measurement

Adaptive readout approaches of resistive sensor array for wearable electronics applications

Zhongliang Zhang [a,b,1], Xiaobin Chen [a,b,1], Lin Shu [a,d,e,*], Xiangmin Xu [a,c,d,e,*]

[a] School of Future Technology, South China University of Technology, Guangzhou 511422, China
[b] School of Microelectronics, South China University of Technology, Guangzhou 511422, China
[c] School of Electronic and Information Engineering, South China University of Technology, Guangzhou 510640, China
[d] Institute of Modern Industrial Technology of SCUT in Zhongshan, Zhongshan, 528400, China
[e] Pazhou Lab, Guangzhou, 510330, China

ARTICLE INFO

Keywords:
Resistive sensor array
Crosstalk error
Readout method
Textile sensor array

ABSTRACT

Sensor arrays are widely used to extract the distribution of variables in large sensing areas or collect multi-degree-of-freedom data. In this paper, we propose adaptive resistance matrix approaches, which can get rid of additional electrical components such as diodes, transistors, multiplexers, op-amps, switches, and current sources. By eliminating the power supply parameters, these approaches can show great advantages and application potential when they are used to measure wearable flexible sensor arrays or other low-cost sensor arrays. Experimental results have shown that the proposed approaches achieved a high accuracy (99.45% and 99.80%), large measurement range (0.5 ~ 1.5 times the reference resistance value), and relatively low crosstalk error (0.066% and 0.128%). The approach was then applied to a flexible strain sensor array to estimate the three-degree-of-freedom lumbar spine motion, and the results have shown that the resistance distribution of the sensor array can clearly show the strain distribution under different lumbar movements.

1. Introduction

Sensor arrays play a critical role in sensing large areas and collecting multi-degree-of-freedom data. Resistive sensor arrays are of interest due to their advantages, such as low complexity, low cost, high stability, high precision, easy integration, etc. Recently, these arrays have been widely used in chemical sensing[1–3], tactile sensing[4–9], imaging [10–13], and man–machine interaction devices[14–16]. However, one of the significant challenges of sensor arrays is the increased number of connecting wires. For example, if each sensor cell requires two wires to read its data, an array of size $m \times n$ requires $2 \times m \times n$ wires. Extensive research has shown that sharing of rows and columns techniques can reduce the number of wires required[17,18]. While some research demonstrated that the shared wires produced many parasitic current paths and seriously affect the readout process, which was called the crosstalk effect[8].

At the moment, a number of methods have been presented to read out the sensor value correctly. Some methods embed diodes or transistors in the sensor array to isolate the parasitic current path, such as the inserting diode method (IDM)[4,5] and the inserting transistor method (ITM)[6,10,19,20]. These methods deteriorate the stretchability, wearability, reliability, and lifetime of flexible sensor arrays due to the embedding of rigid devices. Furthermore, some readout methods attempt to eliminate the crosstalk effect by designing extra readout circuits, such as the passive integrator method (PIM)[8,21,22], the voltage feedback method (VFM)[18,23–26], the zero potential method (ZPM)[27–31], etc. But they need to add additional operational amplifiers, multiplexers, or other devices. Introducing these devices affects their power consumption and cost for large-scale wearable sensor arrays. In addition, some reading methods allow parasitic current to flow in the array because they can extract accurate stimulation signals from computing formulas or deep networks. For example, the incidence matrix approach (IMA)[32] and the resistance matrix approach (RMA)[33]. IMA can extract effective information from crosstalk signals through calculation, which is similar to electrical impedance tomography (EIT) [34–38]. RMA is gradually widely used in low-cost sensor arrays due to its low complexity, satisfactory accuracy, relatively low crosstalk error, sufficient sensor capacity, and no need for additional current sources.

* Corresponding authors.
E-mail addresses: shul@scut.edu.cn (L. Shu), xmxu@scut.edu.cn (X. Xu).
[1] These authors contributed to the work equally and should be regarded as co-first authors.

https://doi.org/10.1016/j.measurement.2023.113524
Received 14 March 2023; Received in revised form 17 August 2023; Accepted 1 September 2023
Available online 2 September 2023
0263-2241/© 2023 The Authors. Published by Elsevier Ltd. This is an open access article under the CC BY-NC-ND license (http://creativecommons.org/licenses/by-nc-nd/4.0/).

However, in practice, the RMA might not guarantee its accuracy, due to the difference between the voltage supplied by the microprocessor and the voltage value fixed in the calculations. The Improved Resistance Matrix Method (IRMA)[39] attempts to reduce the error by measuring the voltage supplied by the microprocessor, and the experimental results demonstrate that IRMA has a smaller measurement error and a wider resistance range than that of RMA. However, it requires more ADC channels and computation resources. This paper proposes adaptive resistance matrix methods (ARMA) to solve this problem without increasing the complexity of the readout circuit and calculation.

The remainder of this article is organized as follows. Section 2 shows the application limitations of RMA. Section 3 presents the details of the derivation process of ARMA and the experimental platform. Section 4 presents the experimental results. Discussions and summary are given in Section 5 and Section 6 respectively.

2. Limitations of RMA

In recent years, there has been an increasing amount of literature using RMA as their readout approach. Using this approach, sensor arrays can be read in a simple and low-cost way. However, RMA calculation is based upon a hypothesis that the power supply voltage provided by the microprocessor is a fixed precise value. In fact, the voltage provided by the microprocessor is usually different from the standard power supply voltage value and is usually fluctuating [40].

Fig. 1 shows the circuit diagram of RMA, it is a resistive sensor array with m rows and n columns, where $R_{1j}(1\leqslant j\leqslant n)$ represents the reference resistance, $ADC_j(1\leqslant j\leqslant n)$ represents the j-th channel of the analog-to-digital converter. The i-th row digital port of the sensor array is represented by p_i in the figure, where $1\leqslant i\leqslant m+1$. By connecting the $m+1$ I/O ports of the microcontroller to the p_1 to p_{m+1} ports of the sensor array, the voltage levels of these ports can be controlled by a microcontroller.

To better understand the mechanisms of RMA and its limitations, a MATLAB program is designed to simulate the calculation error of RMA. In this program, we assume that the voltage set in the RMA calculation equation is Vcc, the voltage supplied by the microcontroller is Vcc^*, all the reference resistance is set to R_{1j}, and all the sensor resistances are set to the same value of R_x. According to the scanning method of the RMA (connect the row that is scanned to the ground and connect other rows to the power source), when the reference resistor row (the first row shown in Fig. 1) is scanned, the voltage value read by the j-th channel of the analog-to-digital converter (ADC) is v_{1j}, which can be represented by

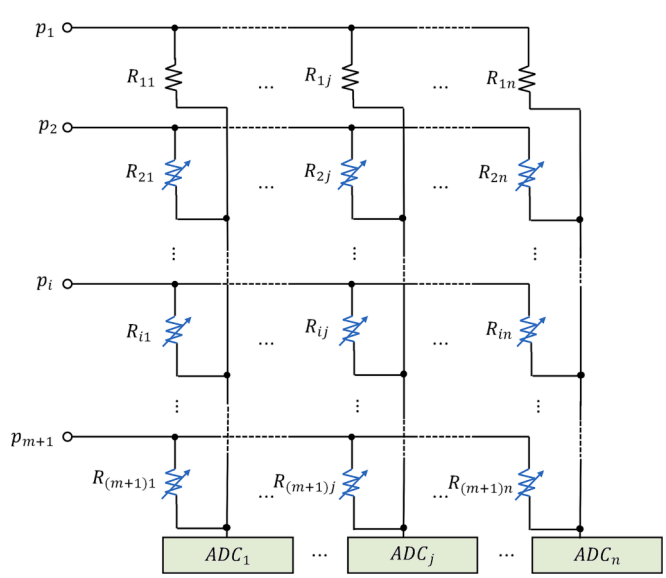

Fig. 1. Sensor array circuit diagram with reference resistor row.

$$v_{1j}=\frac{R_{1j}}{R_{1j}+R_x/m}Vcc^* \tag{1}$$

When row i is scanned, the voltage value read by the j-th channel of the ADC is v_{ij}, which can be represented by

$$v_{ij}=\frac{R_x}{R_x+\frac{R_{1j}\times R_x/(m-1)}{R_{1j}+R_x/(m-1)}}Vcc^* \tag{2}$$

Bring equation (1) and equation (2) into the RMA resistance calculation equation (3)[33], the RMA calculation error can be obtained as shown in equation (4) as a function of the voltage supplied by the microcontroller and different array resistance values.

$$R_{ij}=\frac{\frac{v_{ij}}{Vcc-v_{ij}}+1}{\frac{v_{1j}}{Vcc-v_{1j}}+1}R_{1j}=\frac{Vcc-v_{1j}}{Vcc-v_{ij}}R_{1j} \tag{3}$$

$$Error=\left|\frac{R_{ij}-R_x}{R_x}\right|=\left|\frac{\left(Vcc-\frac{R_{1j}}{R_{1j}+R_x/m}Vcc^*\right)\times R_{1j}}{\left(Vcc-\frac{R_x}{R_x+\frac{R_{1j}\times R_x/(m-1)}{R_{1j}+R_x/(m-1)}}Vcc^*\right)\times R_x}-1\right| \tag{4}$$

By setting $m=n=4$, $R_{1j}=940$, $Vcc=3.3$, the curves of the error changing with the array resistance value under each voltage supplied by the microcontroller can be obtained as shown in Fig. 2.

It can be seen from Fig. 2 that the RMA calculation errors appear to be positively related to the deviation of Vcc^* and Vcc, as when Vcc^* is close to Vcc, the power supply voltage provided by the microprocessor is not much different from the value set in the calculation formula, and the calculation error is minimal. Assuming that we take some measures to minimize this deviation, such as using a regulated power supply to fix the value of the supplied power supply voltage to the value in the formula or using an ADC to monitor the value of the supply voltage supplied by the microprocessor in real time, the readout system's complexity, power consumption, and cost will increase. If we do not take the above efforts, the calculation error of RMA appears to be positively related to the deviation of R_x and R_{1j}. In this case, the setting of the reference resistor value is critical, similar to the electronic interface shown in Ref [41], which requires careful selection of the reference resistor value.

3. Methodology

New adaptive matrix approaches, named Resistance Matrix Approach with Increased scanning times (INCRMA) and Resistance Matrix Approach with Inverting elements in scanning matrix (INVRMA), are proposed. The circuit diagram of these methods is the same as RMA, as shown in Fig. 1.

3.1. Resistance matrix approach with increasing scanning times (INCRMA)

The INCRMA voltage scanning combination matrix S1 can be expressed as equation (5).

$$S1=[e_1\quad e_2^{'}\quad e_2^{''}\quad e_3^{'}\quad e_3^{''}\quad\cdots\quad e_i^{'}\quad e_i^{''}\quad\cdots\quad e_{m+1}^{'}\quad e_{m+1}^{''}] \tag{5}$$

Every element e in S1 is an $(m+1)\times 1$ vector, which represents a single scanning operation, where the zero voltage (0) and high voltage(1) are given to the $m+1$ ports of the sensor array (p_1 to p_{m+1}). Here, the subscript of e corresponds not to the column of S1, but to the i-th row of the sensor array circuit, as shown in Fig. 1. e_1 represents that the first row of the sensor array is given zero voltage value of ground and the

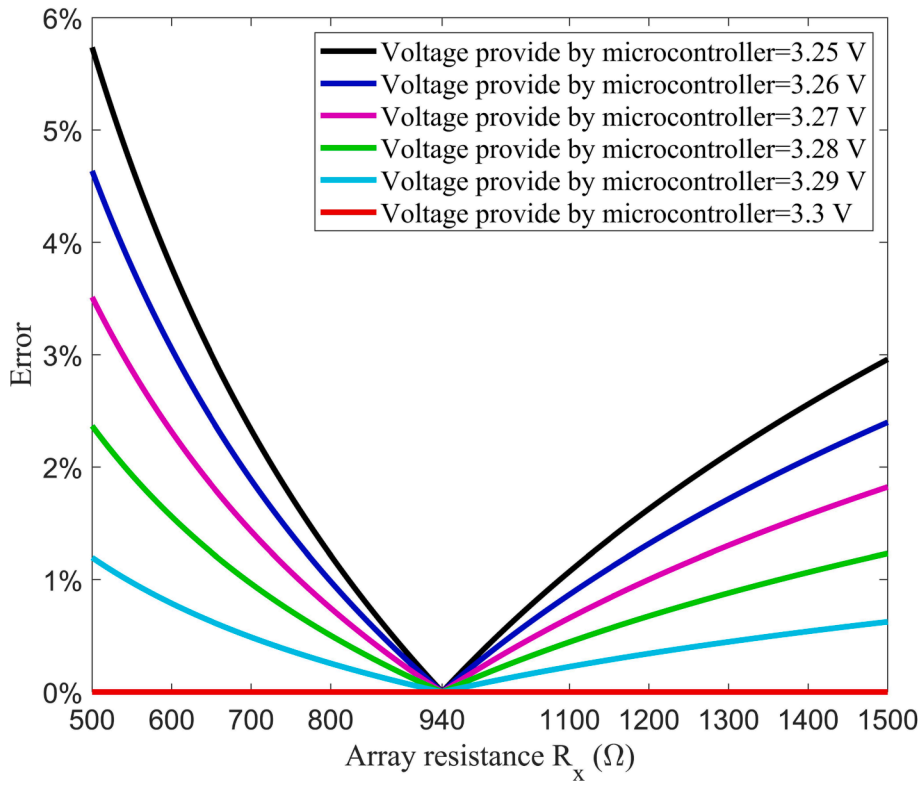

Fig. 2. The error function with Vcc^* and R_x.

other rows are given high voltage values of Vcc^* (Vcc^* is the voltage provided by the microcontroller), $e_i^{'}$ represents that the i-th row is given zero voltage value and the other rows are given high voltage values of Vcc^*. $e_i^{''}$ represents that the first row and the i-th row are given zero voltage values and the other rows are given high voltage values of Vcc^*. S1 is a scanning matrix that contains all the voltage combination vectors used to scan a sensor array. The S1 matrix has $m+1$ rows and $2m+1$ columns.

e_1 can be expressed as equation (6), where 1 represents being connected to the power supply voltage and 0 represents being connected to the ground.

$$e_1 = [0 \quad 1 \quad \cdots \quad 1 \quad \cdots \quad 1]^T \tag{6}$$

The scanning vector $e_i^{'}$ can be expressed by equation (7), where the i-th element (p_i) is 0 and others ($p_2 \sim p_{i-1}$ and $p_{i+1} \sim p_{m+1}$) is 1.

$$e_i^{'} = [1 \quad p_2 \quad \cdots \quad p_i \quad \cdots \quad p_{m+1}]^T \tag{7}$$

In the same way, the scanning vector $e_i^{''}$ can be expressed by equation (8), where the i-th element (p_i) is 0 and others ($p_2 \sim p_{i-1}$ and $p_{i+1} \sim p_{m+1}$) is 1.

$$e_i^{''} = [0 \quad p_2 \quad \cdots \quad p_i \quad \cdots \quad p_{m+1}]^T \tag{8}$$

The difference between $e_i^{'}$ and $e_i^{''}$ is reflected in the first row, $e_i^{'}$ is 1 and $e_i^{''}$ is 0, so the scanning mode of $e_i^{''}$ is equivalent to grounding the reference resistor row in the scanning mode of $e_i^{'}$.

The calculation equation of R_{ij} under e_1 and $e_i^{'}$ is given in (9) [33], and it can be transformed into an equation that can be used to describe Vcc, which is represented by equation (10).

$$R_{ij} = \frac{\frac{v_{ij}}{Vcc-v_{ij}}+1}{\frac{v_{1j}}{Vcc-v_{1j}}+1}R_{1j} = \frac{Vcc-v_{1j}}{Vcc-v_{ij}}R_{1j} \tag{9}$$

$$Vcc = \frac{R_{ij}v_{ij} - R_{1j}v_{1j}}{R_{ij} - R_{1j}} \tag{10}$$

The calculation equation of R_{ij} under e_1 and $e_i^{''}$ is given in equation (11). To distinguish this combination of vectors from the previous combination of vectors, the voltage values read by the ADC in this combination will be marked with an asterisk.

$$R_{ij} = \frac{Vcc\left(Vcc - v_{1j}\right)}{v_{1j}\left(Vcc - v_{ij}^*\right) - v_{ij}^*\left(Vcc - v_{1j}\right)}R_{1j} \tag{11}$$

Using equation (10) and equation (11), equation (12) can be obtained. It is worth noting that the supply voltage has been eliminated in this equation.

$$R_{ij}^2\frac{v_{1j} - v_{ij}^*}{R_{1j}} + R_{ij}\left(v_{ij}^* - v_{ij}\right) = 0 \tag{12}$$

Due to the physical meaning of R_{ij} (R_{ij} can't be zero), the solution of the equation (12) about R_{ij} is shown in the equation (13).

$$R_{ij} = \frac{v_{ij} - v_{ij}^*}{v_{1j} - v_{ij}^*}R_{1j} \tag{13}$$

A solution without the supply voltage parameter in the equation can be obtained, as shown in equation (14). It is worth noting that this calculation formula does not contain any power supply voltage parameters, which guarantees there is no interferences from the power supply in this sensor array.

$$\begin{bmatrix} R_{21} & \cdots & R_{2j} & \cdots & R_{2n} \\ \vdots & \ddots & \vdots & \ddots & \vdots \\ R_{i1} & \cdots & R_{ij} & \cdots & R_{in} \\ \vdots & \ddots & \vdots & \ddots & \vdots \\ R_{(m+1)1} & \cdots & R_{(m+1)j} & \cdots & R_{(m+1)n} \end{bmatrix} = \begin{bmatrix} \frac{v_{21}-v_{21}^*}{v_{11}-v_{21}^*}R_{11} & \cdots & \frac{v_{2j}-v_{2j}^*}{v_{1j}-v_{2j}^*}R_{1j} & \cdots & \frac{v_{2n}-v_{2n}^*}{v_{1n}-v_{2n}^*}R_{1n} \\ \vdots & \ddots & \vdots & \ddots & \vdots \\ \frac{v_{i1}-v_{i1}^*}{v_{11}-v_{i1}^*}R_{11} & \cdots & \frac{v_{ij}-v_{ij}^*}{v_{1j}-v_{ij}^*}R_{1j} & \cdots & \frac{v_{in}-v_{in}^*}{v_{1n}-v_{in}^*}R_{1n} \\ \vdots & \ddots & \vdots & \ddots & \vdots \\ \frac{v_{(m+1)1}-v_{(m+1)1}^*}{v_{11}-v_{(m+1)1}^*}R_{11} & \cdots & \frac{v_{(m+1)j}-v_{(m+1)j}^*}{v_{1j}-v_{(m+1)j}^*}R_{1j} & \cdots & \frac{v_{(m+1)n}-v_{(m+1)n}^*}{v_{1n}-v_{(m+1)n}^*}R_{1n} \end{bmatrix} \tag{14}$$

3.2. Resistance matrix approach with inverting elements in scanning matrix (INVRMA)

Based on the circuit connection in Fig. 1, we adopted the voltage scanning matrix as equation (15). This scanning matrix equals the complement of the scanning matrix of RMA, it can be obtained by inverting each element in the scanning matrix of RMA. As shown in the scanning matrix, each column of S2 sequentially scans each row in the array, that is, each row is sequentially connected to the power source. For example, when row i of the array is scanned, row i will be connected to the supply voltage, while the other rows will be connected to the ground.

$$S2 = \begin{bmatrix} 1 & 0 & \cdots & 0 & \cdots & 0 \\ 0 & 1 & \cdots & 0 & \cdots & 0 \\ 0 & 0 & \ddots & \vdots & \ddots & \vdots \\ \vdots & \vdots & \cdots & 1 & \cdots & 0 \\ 0 & 0 & \ddots & \vdots & \ddots & \vdots \\ 0 & 0 & \cdots & 0 & \cdots & 1 \end{bmatrix} \tag{15}$$

Under the scanning of matrix S2, we can list the Kirchoff's law equation for the column j as shown in equation (16).

$$\begin{bmatrix} 1 & d_{1j} & \cdots & d_{1j} & \cdots & d_{1j} \\ d_{2j} & 1 & \cdots & d_{2j} & \cdots & d_{2j} \\ \vdots & \vdots & \ddots & \vdots & \ddots & \vdots \\ d_{ij} & d_{ij} & \cdots & 1 & \cdots & d_{ij} \\ \vdots & \vdots & \ddots & \vdots & \ddots & \vdots \\ d_{(m+1)j} & d_{(m+1)j} & \cdots & d_{(m+1)j} & \cdots & 1 \end{bmatrix} \begin{bmatrix} 1/R_{1j} \\ 1/R_{2j} \\ \vdots \\ 1/R_{ij} \\ \vdots \\ 1/R_{(m+1)j} \end{bmatrix} = \begin{bmatrix} 0 \\ 0 \\ \vdots \\ 0 \\ \vdots \\ 0 \end{bmatrix} \tag{16}$$

Where $d_{ij} = -\frac{v_{ij}}{V_{cc}-v_{ij}}$, v_{ij} is the voltage measured by ADC_j when $p_i = 1$ and others are 0, that is the situation when row i is scanned. Calculating R_{ij} requires extracting two equations (17) and (18) from equation (16)

$$\frac{1}{R_{1j}} = \frac{v_{1j}}{V_{cc}-v_{1j}}\left(\frac{1}{R_{2j}} + \frac{1}{R_{3j}} + \cdots + \frac{1}{R_{(m+1)j}}\right) \tag{17}$$

$$\frac{1}{R_{ij}} = \frac{v_{ij}}{V_{cc}-v_{ij}}\left(\frac{1}{R_{1j}} + \frac{1}{R_{2j}} + \cdots + \frac{1}{R_{(i-1)j}} + \frac{1}{R_{(i+1)j}} + \cdots + \frac{1}{R_{(m+1)j}}\right) \tag{18}$$

Equation (19) is then obtained.

$$\frac{1}{R_{ij}} - \frac{1}{R_{1j}} = \frac{1}{R_{1j}}\left(\frac{V_{cc}-v_{1j}}{v_{1j}}\right) - \frac{1}{R_{ij}}\left(\frac{V_{cc}-v_{ij}}{v_{ij}}\right) \tag{19}$$

Finally, as shown in equation (20), we can get the expression of R_{ij}.

$$R_{ij} = \frac{v_{1j}}{v_{ij}}R_{1j} \tag{20}$$

The solution of the sensor array can be calculated by equation (21).

$$\begin{bmatrix} R_{21} & \cdots & R_{2j} & \cdots & R_{2n} \\ \vdots & \ddots & \vdots & \ddots & \vdots \\ R_{i1} & \cdots & R_{ij} & \cdots & R_{in} \\ \vdots & \ddots & \vdots & \ddots & \vdots \\ R_{(m+1)1} & \cdots & R_{(m+1)j} & \cdots & R_{(m+1)n} \end{bmatrix} = \begin{bmatrix} \frac{v_{11}}{v_{21}}R_{11} & \cdots & \frac{v_{1j}}{v_{2j}}R_{1j} & \cdots & \frac{v_{1n}}{v_{2n}}R_{1n} \\ \vdots & \ddots & \vdots & \ddots & \vdots \\ \frac{v_{11}}{v_{i1}}R_{11} & \cdots & \frac{v_{1j}}{v_{ij}}R_{1j} & \cdots & \frac{v_{1n}}{v_{in}}R_{1n} \\ \vdots & \ddots & \vdots & \ddots & \vdots \\ \frac{v_{11}}{v_{(m+1)1}}R_{11} & \cdots & \frac{v_{1j}}{v_{(m+1)j}}R_{1j} & \cdots & \frac{v_{1n}}{v_{(m+1)n}}R_{1n} \end{bmatrix} \tag{21}$$

The solution of INVRMA also does not contain any power voltage parameter, indicating that INVRMA can adapt to different supply voltages automatically.

3.3. Experimental platform

To evaluate the practical performance of the above methods on a wearable electronic array, a printed circuit board (PCB) was fabricated, as shown in Fig. 3 (a). The adjustable resistors (3296 W, BAOTER) were used to simulate the different resistance distributions of the sensor array. A multimeter (Keithley 2700, Tektronix), with an accuracy of 0.02%, was used to measure the value of each adjustable resistor. For further explanation, labels are defined to distinguish the adjustable resistance in different locations, as shown in the right part of Fig. 3 (a). There was a five-row and four-column resistor array on the PCB testing board, where the first row of the resistor array (R_{1j}, $1 \leqslant j \leqslant 4$) acted as the reference resistors, while the other four rows (R_{ij}, $2 \leqslant i \leqslant 5$, $1 \leqslant j \leqslant 4$) were used to simulate the sensor resistances. The ARMA calculation algorithm was implemented on the microprocessor (STM32F103ZET6, STMicroelectronics). The resolution and clock of the ADC channels are 12-bit, and 12 MHz respectively, and the voltage sampling time were set to 71.5 × ADC clock. The connection between the PCB board and the microprocessor is shown in Fig. 3(b). The microprocessor was connected to the computer through the serial port. On the computer side, we used a serial port reading program written in python to display the heat map in real-time and save data at a frequency of 10 Hz. Fig. 3(c) shows the thermal map and relative resistance change curves.

Fig. 4 (a) is used to describe the INCRMA calculation. Firstly, we give the reference resistance row zero voltage value of ground and the other rows high voltage values of Vcc^* using the STM32F103ZET6 as shown in Fig. 3 (b), so that the ADCs can be used to collect the voltage value v_{1j} by repeating reading the voltage at the j-th column of the sensor array for 20 times, and taking the average. Then the i-th row of the sensor array is given zero voltage value of ground and the other rows are given high

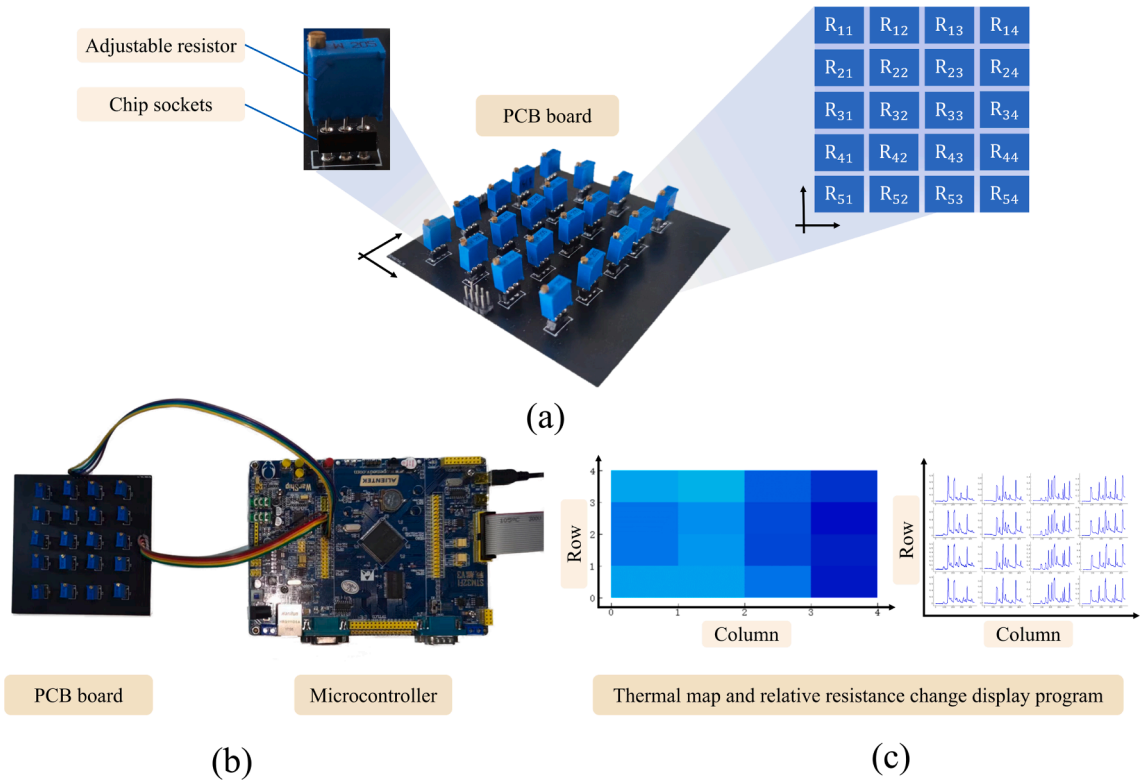

Fig. 3. Experimental platform: (a) PCB board with labels on adjustable resistors. (b) The connection between PCB board and the microcontroller. (c) Thermal map and relative resistance change curves.

voltage values of Vcc^* so that the voltage value v_{ij} can be obtained by repeating reading the voltage at the j-th column of the sensor array for 20 times, and taking the average. After that, we give the reference resistor row and the i-th row of the sensor array zero voltage values of ground and the other rows high voltage values of Vcc^*, so that the voltage value v_{ij}^* can be collected by repeating reading the voltage at the j-th column of the sensor array for 20 times, and taking the average. The value of R_{ij} can then be calculated using the formula of INCRMA. The microprocessor transmits R_{ij} to the PC through the serial port after the calculation is done. On the PC side, the data can be displayed and saved by a python program as shown in Fig. 3 (c). The evaluation of the readout method is done by analyzing the data saved on the PC.

As shown in Fig. 4 (b), INVRMA also has a similar operation process, but the required voltage values are reduced.

1) Accuracy test

To test the accuracy of various reading methods, $R_{ij}(2\leqslant i\leqslant 5, 1\leqslant j\leqslant 4)$ was set to around 1 MΩ and $R_{1j}(1\leqslant j\leqslant 4)$ was set to 940 KΩ as an initial value of the array. The supply voltage value set in the RMA formular was fixed to 3.3 V. To minimize the floating error of the adjustable resistors, we read the value of each adjustable resistor immediately by Keithley after it is adjusted. The resistance measured by Keithley was noted as R_{truth}. We then calculated the error of each approach according to the error calculation equation (22). The average error and the variance of error is calculated by the average and variance of 400 measurement results.

$$Error = \left|\frac{R_{ij} - R_{truth}}{R_{truth}}\right| \tag{22}$$

2) ADC resolution test

To analyze the influence of ADC resolution on the results of the readout method, we assumed that the actual voltage value provided by the microprocessor was around 3.3 V, the reference resistors were all 940 k ohm, the sensor array had four rows and four columns and all the sensor resistances were set to 1 M ohm as their initial values. Then we calculated the voltage values when all the resistance values of the sensor array were adjusted to 50%, 75%, 100%, 125%, and 150% of their initial values. A standard DC voltage source (IT6322A, ITECH) was used to provide these voltages and STM32F407VET6 was used to sample these voltages under different ADC resolutions (8-bit, 10-bit, 12-bit).

3) Measurement range test

For the purpose of comparing the measurement range of RMA and the newly proposed methods, the resistances of the adjustable resistors used to simulate sensor arrays were adjusted to 50%, 75%, 100%, 125%, and 150% of their initial values, and the resistances of reference resistors were fixed at 940 KΩ. We then calculated the average error using the error calculation equation (22) under different adjustment situations.

4) Crosstalk Error Evaluation

The crosstalk error was evaluated by designing four array resistance distribution modes on PCB, as shown below:

Mode 0: set the 16 adjustable resistors in the array around 1 MΩ, and set the reference resistor to 940 KΩ.
Mode 1: randomly select one resistor (except the reference resistor) in the array and change its resistance value to 30% of the previous resistance value in mode 0.
Mode 2: randomly select two resistors (except the reference resistor) and change their resistance value to 30% of the previous resistance value in mode 0.

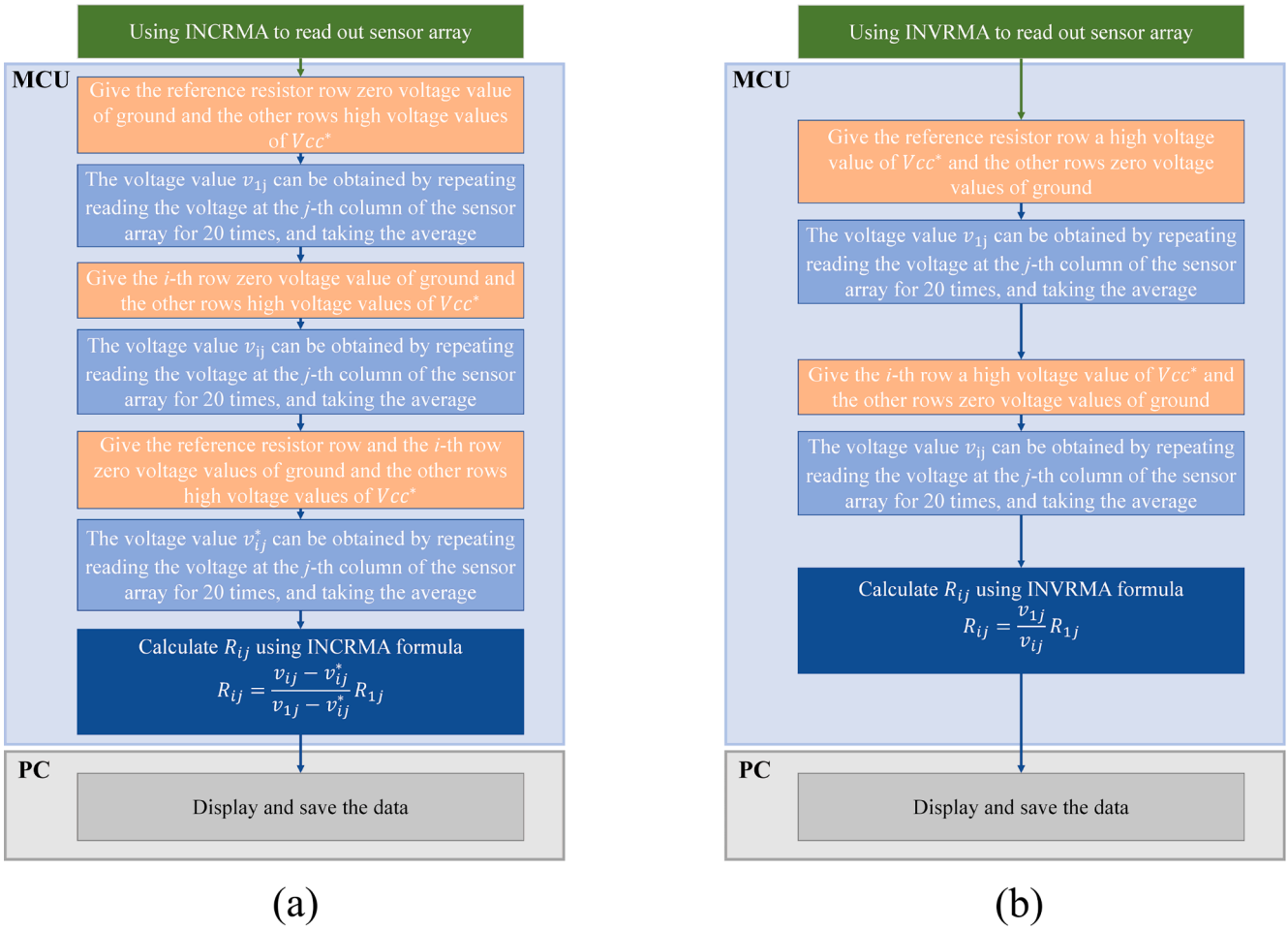

Fig. 4. Flowchart for a single measurement (a) using INCRMA (b) using INVRMA.

Mode 3: randomly select two resistors (except the reference resistor) in the same row and column and change their resistance value to 30% of the previous resistance value in mode 0.

To quantify the effect of changing the selected resistor on the unselected resistors of each method, the coefficient of variation difference (ΔCV) was used as an index. ΔCV could be calculated by subtracting the coefficient of variation (The coefficient of variation is used to compare

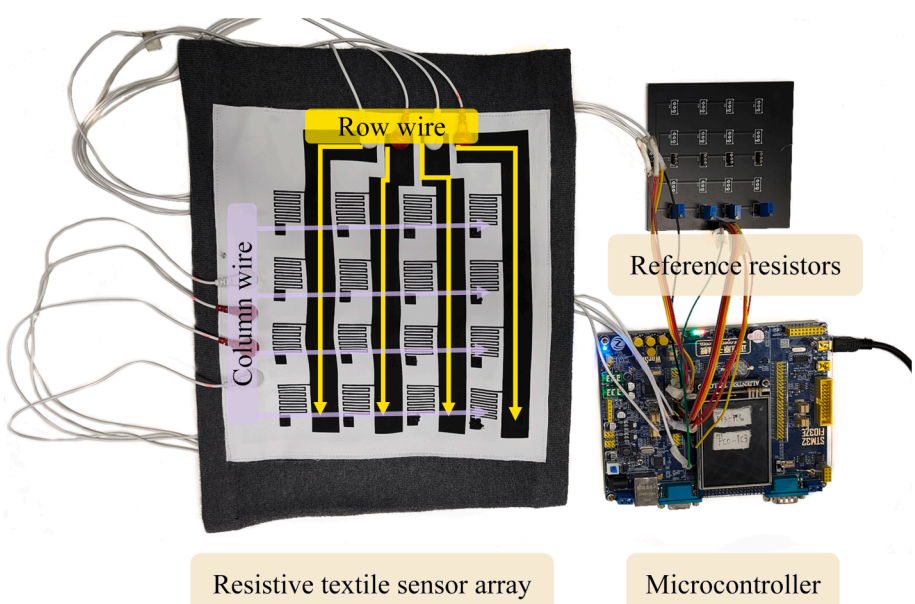

Fig. 5. The prototype of the lumbar spine detection system.

the degree of dispersion of two groups of data, which is the ratio of the standard deviation of the original data to the mean of the original data. The coefficient of variation is a dimensionless quantity) of unselected resistors read in Mode 0 from the coefficient of variation of unselected resistors read in Mode 1 to Mode 3. To enhance the experiment's credibility, the random selection operation of mode 1 to mode 3 was repeated ten times.

5) Application test

Sensor arrays can perceive multi-degree-of-freedom motion than a single sensor. The lumbar pain caused by a long time sitting in an office [42] and irregular working posture[43] often occurs in modern people's work and life. However, the lumbar motion is a three-degree-of-freedom motion[42], and it is hard to be detected by a single sensor. Therefore, lumbar spine movement is a very prospective application scenario for the sensor array.

In this paper, we conducted some preliminary experiments on the feasibility of using a flexible fabric sensor array to detect the motion of the lumbar spine based on ARMA. Detailed information of the resistive textile sensor can be found in Ref [44]. The prototype of the lumbar spine detection system is shown in Fig. 5. In subsequent applications, reference resistors can be integrated with microprocessors to reduce the number of wires and contact impedance.

As for the hysteresis of piezoresistive textile sensor, we conducted an experiment by stretching and releasing strain sensors in the array and record the resistance change. By calculating the average of the loading and unloading curves (relative resistance change vs. strain), a fitted curve was obtained and adopted in the applications. A repeatability test was also conducted. In order to ensure that the stimulus applied to the fabric array was the same, we fixed the flexible fabric array and used a tensile machine to apply a fixed degree of strain stimulation cycle to certain sensor in the array.

In the application experiment, we asked a volunteer to wear flexible strain sensors on the waist and make some postures (T-pose, sagittal flexion, compound posture, axial rotation, lateral bending) that originate from Ref[42]. During the experiments, the volunteer was first required to hold the T-pose for 10 s before moving into other positions. Each position (sagittal flexion, compound posture, axial rotation, and lateral bending) was held for 10 s, and the volunteer was required to return to the T-pose and hold it for 10 s between two different positions. INCRMA was used to read out the resistance distribution at the same time.

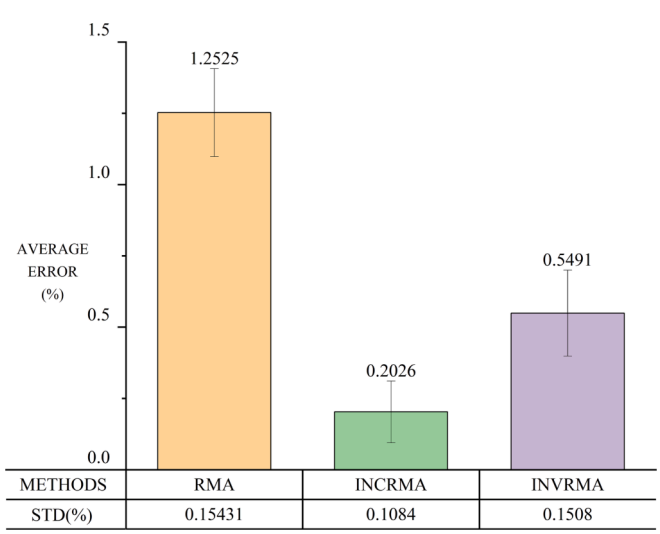

Fig. 6. The average error of 16 resistors for all methods.

4. Results

4.1. Accuracy test results

The average errors of 16 resistors for each method are shown in Fig. 6. It can be seen from Fig. 6 that under this array resistance distribution, INCRMA could control the error of 16 resistors below 0.31% and INVRMA could control the error of 16 resistors below 0.70%, while the error of RMA was between 1.10% and 1.41%. This proves that ARMA has higher accuracy than RMA, and INCRMA exhibits better performance than INVRMA, in this array resistance distribution.

4.2. ADC resolution test results

The errors of different readout approaches are shown in Fig. 7. From the figure, we can see that the resolution of the ADC does not have a large impact on the calculation errors of RMA, INCRMA, and INVRMA, it only causes relatively significant error fluctuations under the two ratios of 50% and 150%, where the error fluctuates around 1% for RMA, 0.5 % for INCRMA, and 1% for INVRMA respectively.

4.3. Measurement range test results

The average errors of various methods under different array resistance distribution values are shown in Fig. 8. When the array resistance deviates from the reference resistance, the maximum error of RMA could reach 13.99%. In comparison, the maximum error of the newly proposed INCRMA method was only 0.39%, and the maximum error of the INVRMA method was only 1.08%.

By connecting the error points of RMA and ARMA under different array resistance distributions, as shown in Fig. 8, it can be found that the closer the resistance value in the array is to the reference resistance value, the lower the RMA calculation error. The explanation for this result is that RMA calculates sensor resistances in the array using *Vcc* parameters, but the high voltage output via the IO port is not exactly the *Vcc* value of 3.3 V, which causes calculation error. For RMA, the calculation errors are also relevant to the measured resistance value R_x, as shown in equation (4). The simulation and experimental results are shown in Fig. 2 and Fig. 8 respectively, where it is observed the measurement range varies among these methods.

The other two methods of INCRMA and INVRMA proposed in this paper do not involve the *Vcc* parameter in the array calculations, so their errors can be lower than RMA in this aspect, which can be observed that the curve of INVRMA and INCRMA can keep smaller errors than RMA under various array resistance distributions.

In addition, the measurement error of ADC also causes errors, which makes the actual testing error of all methods larger than the error calculated by simulation.

4.4. Crosstalk error evaluation results

Boxplots were used to represent the experimental results of RMA, INCRMA, and INVRMA in the 1 to 3 array resistance distribution mode, as shown in Fig. 9.

To compare the performance of three methods on crosstalk, Fig. 9 unifies the vertical axis range from −0.5% to 2.5%. The CV changes of RMA and INVRMA are not significant, so a large amplitude cannot be observed in the figure. The average IQR of RMA, INCRMA, and INVRMA were 0.09%, 0.28%, and 0.08%, respectively, which shows that INCRMA has a higher degree of dispersion than the other two methods. We can also observe this situation from Fig. 9, which shows that the ΔCV distribution range of INCRMA was wider than that of RMA and INVRMA in experiments 6,7,8,9 in mode 1, experiments 1,10 in mode 2, and experiments 1,3,4,5,6 in mode 3. The reason for the relatively large dispersion of INCRMA may due to the fact that its scanning period is $(2m+1)/(m+1)$ times that of other methods, which increases the possibility

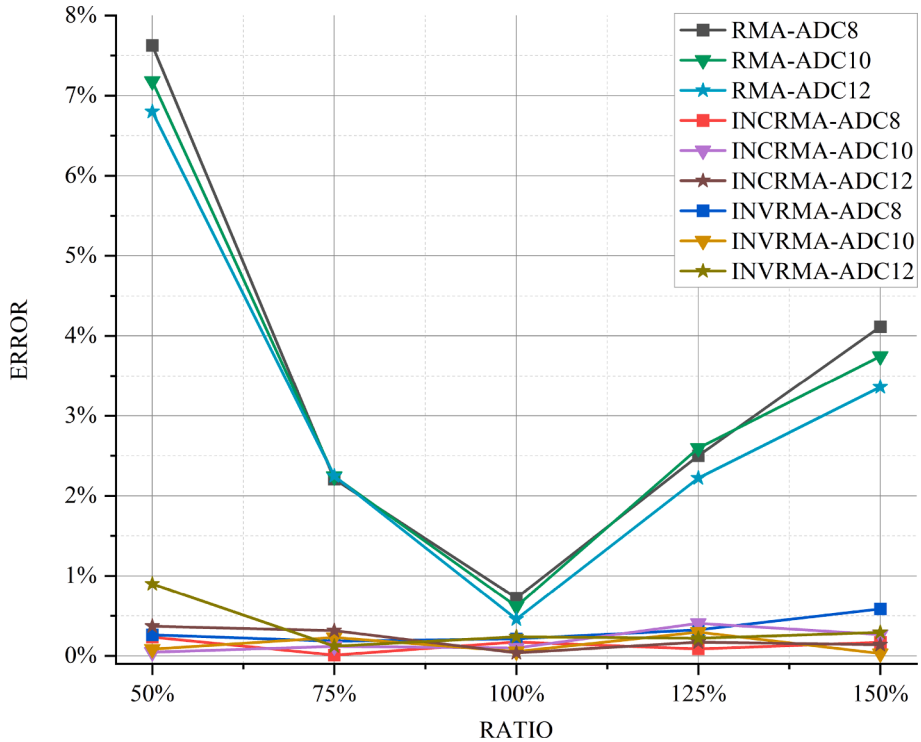

Fig. 7. Error of readout approaches under different ADC resolutions (ADC*x* indicates the use of an *x*-bit ADC, RATIO indicates that the resistance of sensors in the array was adjusted to 50%, 75%, 100%, 125%, and 150% of their initial value).

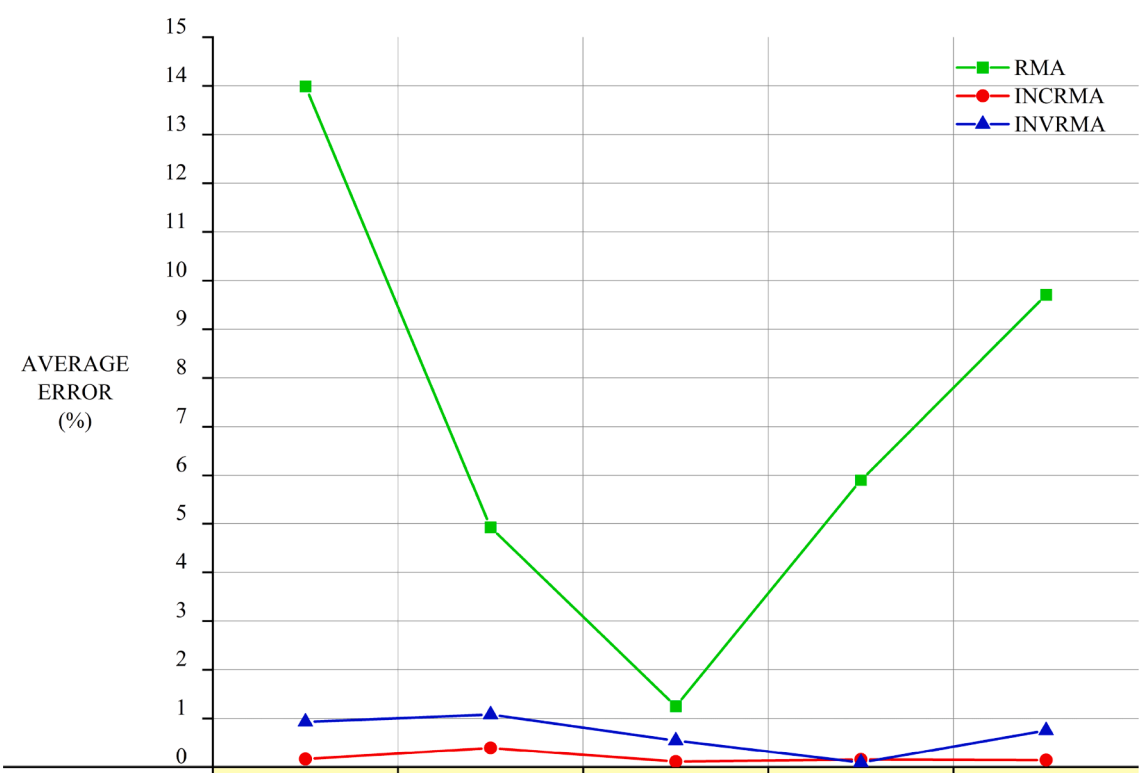

RATIO	50%	75%	100%	125%	150%
RMA	13.99%	4.92%	1.25%	5.90%	9.71%
INCRMA	0.17%	0.39%	0.11%	0.15%	0.14%
INVRMA	0.93%	1.08%	0.55%	0.09%	0.75%

Fig. 8. Measurement range of various methods (RATIO: the resistance of sensors was adjusted to 50%, 75%, 100%, 125%, and 150% of their initial value).

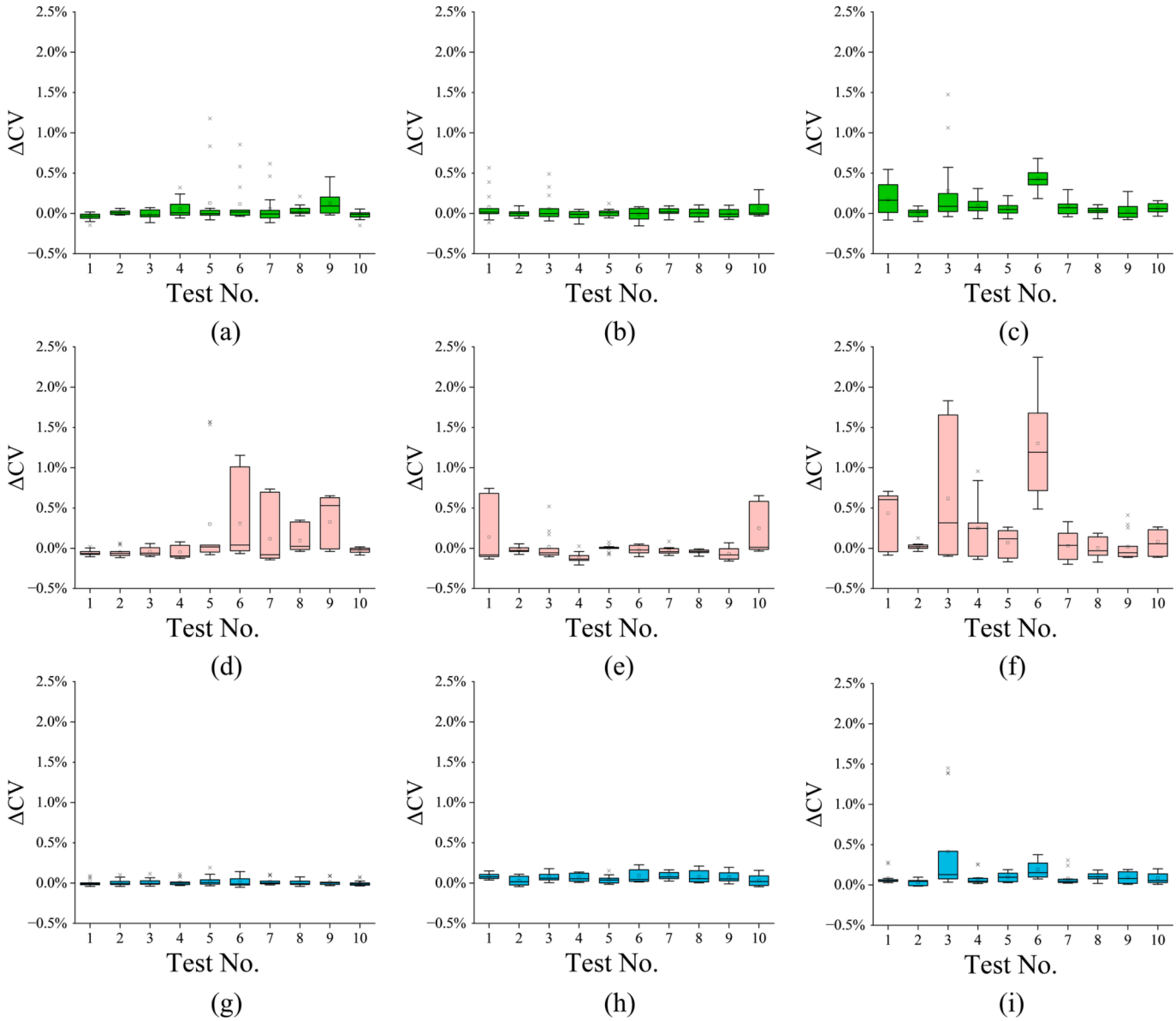

Fig. 9. The box diagram of the crosstalk error evaluation experiment: (a) RMA in Mode 1. (b) RMA in Mode 2. (c) RMA in Mode 3. (d) INCRMA in Mode 1. (e) INCRMA in Mode 2. (f) INCRMA in Mode 3. (g) INVRMA in Mode 1. (h) INVRMA in Mode 2. (i) INVRMA in Mode 3. (Box plot configurations: box range: 25–75%, whisker range: 1.5IQR. meanings of the percentile symbols: '−' refers to the max or min, '−' in the box refers to the median, '×' refers to the outlier, '□' refers to the mean.).

Table 1
Comparison of relevant methods.

Methods		Scanning period	Average error	Measurement range ($Error \leqslant 1.25\%$)	Crosstalk
RMA		$m+1$	1.25%	$\approx Ref$	0.063%
ARMA	INCRMA	$2m+1$	0.20%	$0.5Ref \sim 1.5Ref$	0.128%
	INVRMA	$m+1$	0.55%	$0.5Ref \sim 1.5Ref$	0.066%

of sensor instability and causes fluctuations. The median of the RMA or ARMA was both close to zero in these experiments, which means they both have fewer crosstalk effects.

4.5. Comparison between various methods

When reading a sensor array with m rows and n columns, a detailed comparison of relevant methods is shown in Table 1.

(Scanning period represents the number of voltage sweeps required to calculate all the sensor resistance in the sensor matrix, Ref represents the resistance value of reference resistor, and the crosstalk is represented by the average of ΔCV).

The adaptive resistance matrix approaches all continue the minimalist circuit connection of RMA, which makes these methods have the advantages of low operational complexity, low power consumption of the readout circuit, and no additional power supply. When the power supply voltage parameters were inconsistent with the actual voltage, the average error of the two newly proposed ARMA methods was less than half of that of RMA. For the measurement range, RMA could only ensure relatively low error when the resistance value of the array was close to the reference resistor, while the two ARMA extended the measurement range to 0.5 ∼ 1.5 times of the reference resistance value. From the crosstalk index, we can find that INCRMA has a higher average ΔCV than the other two methods. The average ΔCV for RMA and ARMA were

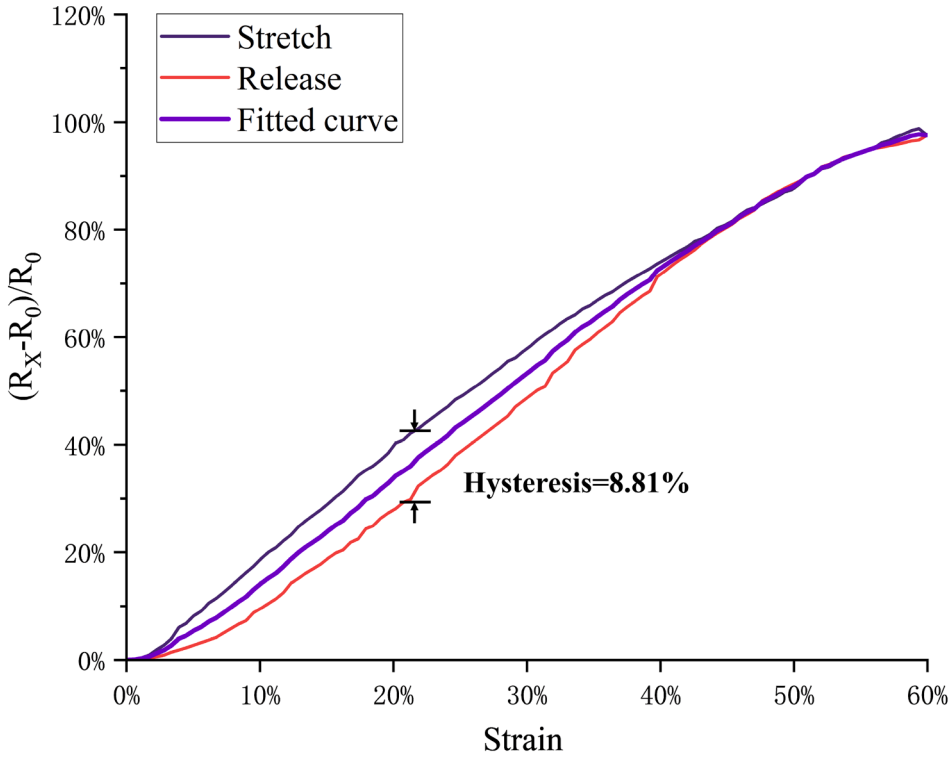

(a)

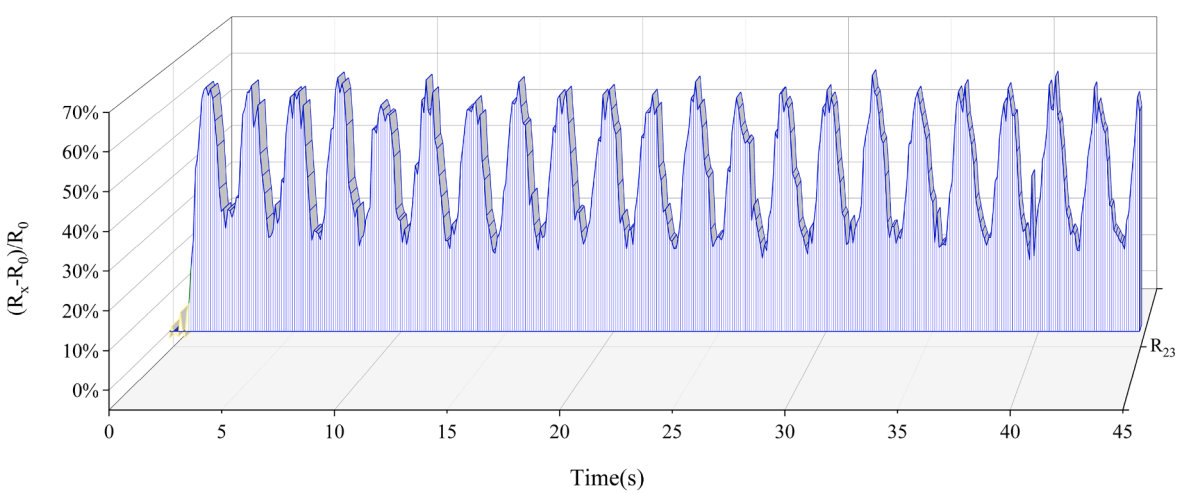

(b)

Fig. 10. (a) The hysteresis curves of the sensors. (b) Repeatability test result. (c) Resistance distribution of flexible fabric array under sagittal flexion and compound gestures. (d) resistance distribution of flexible fabric array under axial rotation and lateral bending.

all smaller than 0.13%, and it is acceptable for a 70% change in resistance. After comprehensively considering the scanning period, the measurement range, the average error, and the crosstalk error, INVRMA might be the best approach. According to the description of IRMA in Ref [39], IRMA has the advantage of a shorter scanning period compared with RMA, INCRMA, and INVRMA. While IRMA increases the consumption of on-chip sampling and computing resources, which may limit its applications.

4.6. Application

As for the hysteresis of piezoresistive textile sensor, the typical curve of a textile sensor is shown in Fig. 10 (a), we can find that the hysteresis of the sensor in was about 8.81%. We used the fitted average curve to calculate the strain from the resistance data, which can reduce hysteresis error by half. Fig. 10 (b) indicates that the sensor had a relatively stable performance.

As for the application experiment, the sagittal flexion action caused the entire array to be stretched, and almost all sensor units exhibited a

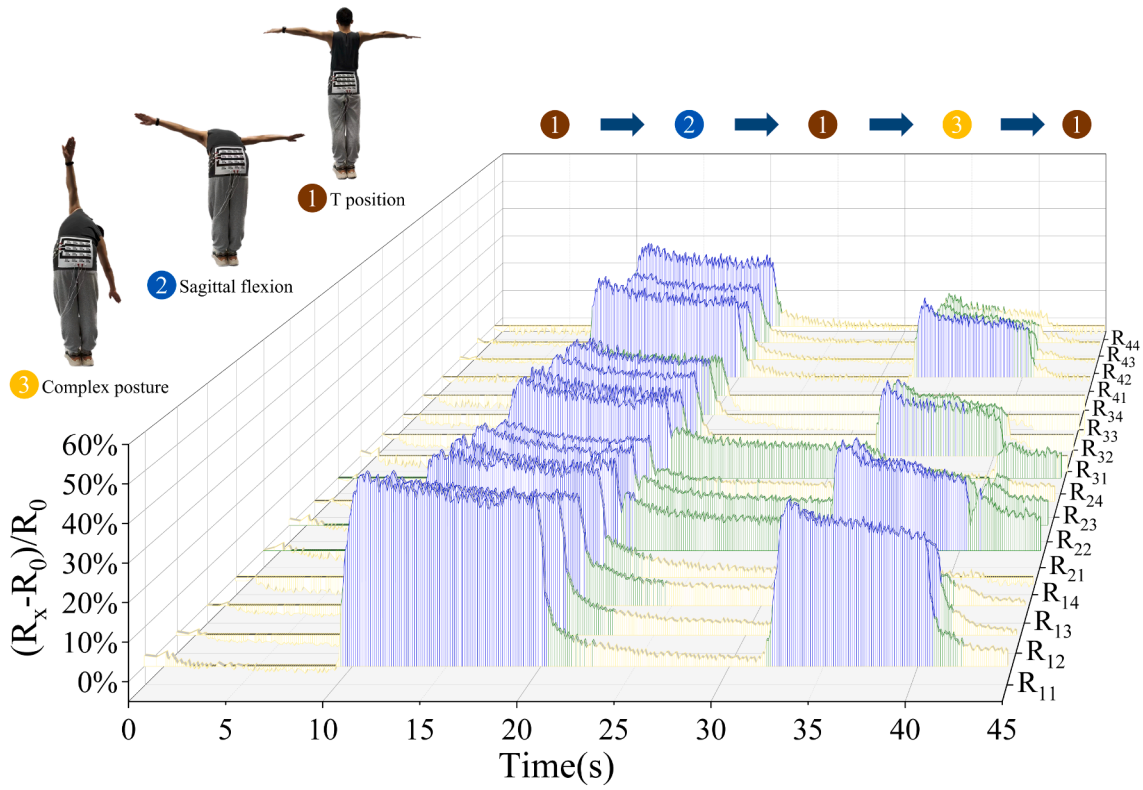

(c)

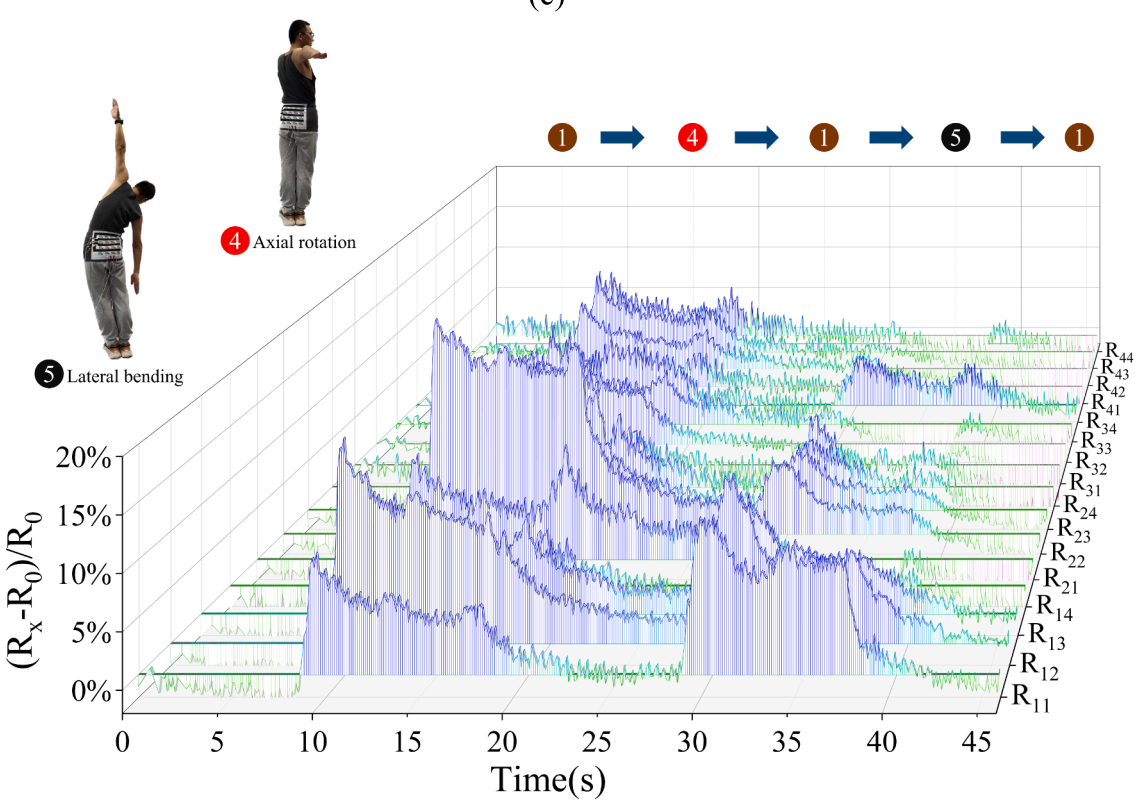

(d)

Fig. 10. (*continued*).

large relative resistance change, as shown in the curve under action 2 in Fig. 10 (c). For compound gestures, the sensors in the first and second columns varied more than those in the third and fourth columns, which is consistent with the fact that action 3 causes greater strain in the left part of the array (R_{11},R_{12},R_{21},R_{22},R_{31},R_{41}). For axial rotation and lateral bending, the relative resistance changes of all the sensors (less than

20%) were smaller than sagittal flexion and compound posture (less than 60%), as shown in Fig. 10 (d). For axial rotation, the sensor in the second row and the second column of the fabric array had a larger relative resistance change than other sensors. For lateral bending, the relative resistance changes of each sensor in each row in the sensor array decreased gradually from column 1 to column 4, which also satisfies the strain condition caused by action 5. In general, the changes of all sensors were consistent with the strain changes caused by posture.

5. Discussions

Here some essential factors of the ARMA are further discussed.

Unstable power supply voltage: When the power supply voltage fluctuates and the scanning frequency is not fast enough, the power supply voltage parameters in all the equations will not be the same, and it causes errors in the process of obtaining a unique solution or eliminating the supply voltage parameters. This error can be reduced by using a faster microcontroller, powering from a regulated voltage source, or regulating the voltage with a capacitor.

Reading speed: The sensor data reading time of these readout approaches (RMA, INVRMA, INCRMA) depends on the GPIO port update time, the reading speed of ADC and the resistance calculation time, as shown in equation (23).

$$T_{read} = T_{GPIO} + T_{ADC} + T_{cal} \tag{23}$$

For example, when we use STM32F10X microprocessor to read a sensor array with m rows and n columns and set GPIO port update frequency at 50 MHz, ADC clock at 12 MHz and the voltage sampling time at 1.5 × ADC clock. As assumed above, the time cost for RMA, INCRMA and INVRMA is shown in equation (24), (25), (26), respectively.

$$T_{RMA} = (3m+1) \times 0.02 \times 10^{-6} + (m+1) \times n \times 14/12 \times 10^{-6} + 22 \times m \times n \times 2 \times 11 \times 10^{-9} \tag{24}$$

$$T_{INCRMA} = (5m+2) \times 0.02 \times 10^{-6} + (2m+1) \times n \times 14/12 \times 10^{-6} + 12 \times m \times n \times 2 \times 11 \times 10^{-9} \tag{25}$$

$$T_{INVRMA} = (3m+1) \times 0.02 \times 10^{-6} + (m+1) \times n \times 14/12 \times 10^{-6} + 6 \times m \times n \times 2 \times 11 \times 10^{-9} \tag{26}$$

If $m = n = 4$, the time cost is 31.34 μs for RMA, 46.66 μs for INCRMA, and 25.71 μs for INVRMA, respectively. The additional scanning time for INCRMA is around 20 μs. In practical applications, this time consumption may vary or even be longer due to different parameter settings. But it is still applicable for wearable applications in daily life as the time cost is at the millisecond or microsecond level.

As for the total readout speed, calculation equation was given below. The real-time performance of this system depends on the sensor data reading time and transmission time, including the GPIO port update time, the reading speed of the ADC, the resistance calculation time, and the data transmission time via serial port, as shown in equation (27).

$$T_{total} = T_{read} + T_{trans} \tag{27}$$

If the baud rate is 115200, the serial port transmission will take $16 \times 4 \times 10/115200 = 5.556$ ms (sending 16 floating-point data). Then the total time for INCRMA is about 5.602 ms. That means we can use 5.6 ms to read the sensor array once, and the frequency can be higher than 100 Hz if we don't consider the data processing time at the host computer. At the computer, as the python program needs to save data and display both heat maps and dynamic curves of the sensor data, it might cost more than 10 ms in these processes. The modules that occupy the main time cost are data transmission and processing at the host computer. Therefore, the speed of this system can be further improved by increasing the data transmission speed, and optimizing the processing program.

Method extensibility: For the method of increasing scanning times to obtain the resistance matrix approach, we can obtain more solutions of this type of method by modifying $e_i^{'}$ and $e_i^{''}$, when we ensure to have a unique solution of R_{ij}.

Measurement error: The measurement error is mainly caused by the ADC, the adjustable resistor, and the conduction wire in this study. Replacing the 12-bit ADC with a 16-bit ADC or using a more standard ADC reference voltage will effectively reduce the error caused by voltage measurement. The resistance value deviation of the resistors due to temperature, humidity, and mechanical vibration might also cause errors. Using more stable resistors and lower resistance wires might effectively reduce measurement errors.

In addition, factors such as the contact resistance between the elastic fabric and the wire, the noise level of signal transmission during human motion, the stability of the resistance value of the fabric array, and human sweat may also affect the accuracy of the measurement. These contents are worth studying in the next stage.

6. Conclusions

The proposed adaptive resistance matrix approaches can be obtained by increasing scanning times or inverting elements in the scanning matrix. The experiment results have shown that the proposed approaches, both INCRMA and INVRMA, have smaller errors and wider measurement ranges than RMA while keeping the circuit complexity unchanged. After comprehensively considering the scanning period, the measurement range, the average error, and the crosstalk error, INVRMA might be the best approach. When the new approach is applied to a flexible fabric sensor array, the experimental results show that the flexible array has different resistance value distributions for different lumbar spine motions. It is worth continuing to study how to eliminate the calculation error caused by the fluctuation of the power supply voltage and how to reduce the noise caused by the increase in the number of scans.

CRediT authorship contribution statement

Zhongliang Zhang: Conceptualization, Methodology, Software, Investigation, Formal analysis, Writing – original draft, Data curation, Visualization. **Xiaobin Chen:** Software, Validation, Investigation, Data curation. **Lin Shu:** Methodology, Writing – review & editing, Funding acquisition, Supervision. **Xiangmin Xu:** Resources, Funding acquisition, Supervision, Project administration.

Declaration of Competing Interest

The authors declare that they have no known competing financial interests or personal relationships that could have appeared to influence the work reported in this paper.

Data availability

Data will be made available on request.

Acknowledgment

This work was sponsored by the National Key R&D Program of China (2022YFB4500600), in part by the CIE-Tencent Robotics X Rhino-Bird Focused Research Program, in part by the Major Science and Technology Projects in Guangdong Province under Grant 2016B010108008, in part by the Technology Programme of Guangzhou under Grants 202002030354 and 202002030262, in part by the Science and

Technology Project of Zhongshan under Grants 2019AG024 and 2020B2053, in part by the Natural Science Foundation of Guangdong Province under Grant 2018A030310407, in part by the Guangzhou Key Laboratory of Body Data Science under Grant 201605030011, in part by the Guangdong Provincial Key Laboratory of Human Digital Twin under Grant 2022B1212010004, in part by the National Natural Science Foundation of China under Grants 61972163 and 61806210, and the National Natural Science Foundation of China (Grant No. T2192931).

REFERENCES

[1] A. Depari, M. Falasconi, A. Flammini, D. Marioli, S. Rosa, S. Rosa, S. Rosa, S. Rosa, S. Rosa, G. Sberveglieri, A. Taroni, A. Taroni, A new low-cost electronic system to manage resistive sensors for gas detection, IEEE Sens. J. (2007), https://doi.org/10.1109/jsen.2007.895965.

[2] R. Beccherelli, I. Fratoddi, E. Zampetti, S. Pantalei, M. Bernabei, K.C. Persaud, Design of a very large chemical sensor system for mimicking biological olfaction, Sensors and Actuators B-Chemical. (2010), https://doi.org/10.1016/j.snb.2009.11.031.

[3] M.T. Grassi, P. Malcovati, A. Baschirotto, A high-precision wide-range front-end for resistive gas sensors arrays, Sensors and Actuators B-Chemical. (2005), https://doi.org/10.1016/j.snb.2005.03.103.

[4] D. Prutchi, M. Arcan, Dynamic contact stress analysis using a compliant sensor array, Measurement (1993), https://doi.org/10.1016/0263-2241(93)90039-k.

[5] W.E. Snyder, J.S. Clair, Conductive elastomers as sensor for industrial parts handling equipment, IEEE Trans. Instrum. Meas. (1978), https://doi.org/10.1109/tim.1978.4314628.

[6] B.J. Kane, M.R. Cutkosky, G.T.A. Kovacs, A traction stress sensor array for use in high-resolution robotic tactile imaging, IEEE/ASME, J. Microelectromech. Syst. (2000), https://doi.org/10.1109/84.896763.

[7] T.H. Speeter, Flexible, Piezoresistive Touch Sensing Array, in: D.J. Svetkoff (Ed.), Optics, Illumination, and Image Sensing for Machine Vision III, SPIE, 1989, pp. 31–43, https://doi.org/10.1117/12.949024.

[8] F. Vidal-Verdú, Ó. Oballe-Peinado, J.A. Sánchez-Durán, J. Castellanos-Ramos, R. Navas-González, Three realizations and comparison of hardware for piezoresistive tactile sensors, Sensors. (2011), https://doi.org/10.3390/s110303249.

[9] B. Tise, A compact high resolution piezoresistive digital tactile sensor, In: 1988 IEEE International Conference on Robotics and Automation Proceedings, 1988: pp. 760–764 vol.2. https://doi.org/10.1109/ROBOT.1988.12150.

[10] A. Tanaka, S. Matsumoto, S. Matsumoto, N. Tsukamoto, N. Tsukamoto, S. Itoh, S. Itoh, K. Chiba, K. Chiba, T. Endoh, T. Endoh, A. Nakazato, A. Nakazato, K. Okuyama, K. Okuyama, Y. Kumazawa, M. Hijikawa, M. Hijikawa, H. Gotoh, H. Gotoh, T. Tanaka, N. Teranishi, Infrared focal plane array incorporating silicon IC process compatible bolometer, IEEE Trans. Electron Devices (1996), https://doi.org/10.1109/16.543017.

[11] S. Wang, M. Berentsen, T. Kaiser, Signal processing algorithms for fire localization using temperature sensor arrays, Fire Saf. J. (2005), https://doi.org/10.1016/j.firesaf.2005.06.004.

[12] R. Saxena, R. Bhan, C. Jalwania, S. Lomash, A novel test structure for process control monitor for un-cooled bolometer area array detector technology, J. Semicond. Technol. Sci. 6 (2006) 299.

[13] R.S. Saxena, A. Panwar, S.K. Semwal, P.S. Rana, S. Gupta, R.K. Bhan, PSPICE circuit simulation of microbolometer infrared detectors with noise sources, Infrared Phys. Technol. (2012), https://doi.org/10.1016/j.infrared.2012.07.004.

[14] J. Wu, L. Wang, J. Li, A handwriting input method based on the thermal cue of the fingertip, Measurement (2016), https://doi.org/10.1016/j.measurement.2016.05.097.

[15] M.-Y. Cheng, W.-Y. Chang, L.-C. Tsao, S.-A. Yang, Y.-J. Yang, W.-P. Shih, F.-Y. Chang, S.-H. Chang, K.-C. Fan, Design and fabrication of an artificial skin using PI-copper films, in: 2007 IEEE 20th International Conference on Micro Electro Mechanical Systems (MEMS), 2007, pp. 389–392, https://doi.org/10.1109/MEMSYS.2007.4433149.

[16] P. Parzer, A. Sharma, A. Vogl, J. Steimle, A. Olwal, M. Haller, SmartSleeve: real-time sensing of surface and deformation gestures on flexible, interactive textiles, using a hybrid gesture detection pipeline, in: Proceedings of the 30th Annual ACM Symposium on User Interface Software and Technology, Association for Computing Machinery, New York, NY, USA, 2017, pp. 565–577, https://doi.org/10.1145/3126594.3126652.

[17] R.S. Saxena, N.K. Saini, R.K. Bhan, Analysis of crosstalk in networked arrays of resistive sensors, IEEE Sensors J. 11 (2011) 920–924, https://doi.org/10.1109/JSEN.2010.2063699.

[18] J. Wu, L. Wang, J. Li, Design and crosstalk error analysis of the circuit for the 2-D networked resistive sensor array, IEEE Sens. J. (2015), https://doi.org/10.1109/jsen.2014.2359967.

[19] K. Takei, T. Takahashi, J.C. Ho, H. Ko, A.G. Gillies, P.W. Leu, R.S. Fearing, A. Javey, Nanowire active-matrix circuitry for low-voltage macroscale artificial skin, Nat. Mater. (2010), https://doi.org/10.1038/nmat2835.

[20] C. Wang, D.J. Hwang, Z. Yu, K. Takei, J. Park, T. Chen, B. Ma, A. Javey, User-interactive electronic skin for instantaneous pressure visualization, Nat. Mater. (2013), https://doi.org/10.1038/nmat3711.

[21] Ó. Oballe-Peinado, F. Vidal-Verdú, J.A. Sánchez-Durán, J. Castellanos-Ramos, J. A. Hidalgo-López, Accuracy and resolution analysis of a direct resistive sensor array to FPGA interface, Sensors (2016), https://doi.org/10.3390/s16020181.

[22] Ó. Oballe-Peinado, F. Vidal-Verdú, J.A. Sánchez-Durán, J. Castellanos-Ramos, J. A. Hidalgo-López, Improved circuits with capacitive feedback for readout resistive sensor arrays, Sensors (2016), https://doi.org/10.3390/s16020149.

[23] W. Jianfeng, W. Lei, J. Li, Z. Yu, A small size device using temperature sensor array, Chin. J. Sens. Actuators 24 (2011) 1649–1652, https://doi.org/10.3969/j.issn.1004-1699.2011.11.026.

[24] H. Liu, H. Liu, H. Liu, Y.-F. Zhang, Y. Zhang, L. Yiwei, Y. Liu, M. Jin, Measurement errors in the scanning of resistive sensor arrays, Sensors and Actuators A-Physical. (2010), https://doi.org/10.1016/j.sna.2010.08.004.

[25] T. D'Alessio, Measurement errors in the scanning of piezoresistive sensors arrays, Sensors and Actuators A-Physical. (1999), https://doi.org/10.1016/s0924-4247(98)00204-0.

[26] J. Wu, L. Wang, L. Wang, L. Wang, J. Li, J. Li, General voltage feedback circuit model in the two-dimensional networked resistive sensor array, Journal of Sensors. (2015), https://doi.org/10.1155/2015/913828.

[27] R. Lazzarini, R. Magni, P. Dario, A tactile array sensor layered in an artificial skin, in: Proceedings 1995 IEEE/RSJ International Conference on Intelligent Robots and Systems. Human Robot Interaction and Cooperative Robots vol. 3, 1995, pp. 114–119, https://doi.org/10.1109/IROS.1995.525871.

[28] R.S. Saxena, R.K. Bhan, N.K. Saini, R. Muralidharan, Virtual ground technique for crosstalk suppression in networked resistive sensors, IEEE Sens. J. (2011), https://doi.org/10.1109/jsen.2010.2060186.

[29] R. Yarahmadi, A. Safarpour, R. Lotfi, An improved-accuracy approach for readout of large-array resistive sensors, IEEE Sens. J. (2016), https://doi.org/10.1109/jsen.2015.2477494.

[30] J. Wu, J. Li, Approximate model of zero potential circuits for the 2-D networked resistive sensor array, IEEE Sens. J. (2016), https://doi.org/10.1109/jsen.2016.2530692.

[31] J.-S. Kim, D.-Y. Kwon, B.-D. Choi, High-accuracy, compact scanning method and circuit for resistive sensor arrays, Sensors (2016), https://doi.org/10.3390/s16020155.

[32] F. Lorussi, W. Rocchia, E.P. Scilingo, A. Tognetti, D.D. Rossi, Wearable, redundant fabric-based sensor arrays for reconstruction of body segment posture, IEEE Sens. J. (2004), https://doi.org/10.1109/jsen.2004.837498.

[33] Lin Shu, Xiaoming Tao, D.D. Feng, A new approach for readout of resistive sensor arrays for wearable electronic applications, IEEE Sensors J. 15 (2015) 442–452, https://doi.org/10.1109/JSEN.2014.2333518.

[34] N. Li, H. Xu, Z. Zhou, J. Xin, Z. Sun, X. Xu, Reconfigurable bioimpedance emulation system for electrical impedance tomography system validation, IEEE Trans. Biomed. Circuits Syst. (2013), https://doi.org/10.1109/tbcas.2012.2224110.

[35] A.S. Tucker, R. Fox, R. Fox, R. Fox, R.J. Sadleir, Biocompatible, high precision, wideband, improved howland current source with lead-lag compensation, IEEE Trans. Biomed. Circuits Syst. (2013), https://doi.org/10.1109/tbcas.2012.2199114.

[36] H. Alirezaei, A. Nagakubo, Y. Kuniyoshi, A highly stretchable tactile distribution sensor for smooth surfaced humanoids, in: 2007 7th IEEE-RAS International Conference on Humanoid Robots, IEEE, Pittsburgh, PA, USA, 2007, pp. 167–173, https://doi.org/10.1109/ICHR.2007.4813864.

[37] Y. Kato, T. Mukai, T. Hayakawa, T. Shibata, Tactile sensor without wire and sensing element in the tactile region based on EIT method, IEEE SENSORS 2007 (2007) 792–795, https://doi.org/10.1109/ICSENS.2007.4388519.

[38] H. Alirezaei, A. Nagakubo, Y. Kuniyoshi, A Tactile Distribution Sensor Which Enables Stable Measurement Under High and Dynamic Stretch, In: K. Kiyokawa, S. Coquillart, R. Balakrishnan (Eds.), 3DUI : IEEE SYMPOSIUM ON 3D USER INTERFACES 2009, PROCEEDINGS, IEEE; IEEE Comp Soc; IEEE, VGTC, 2009: p. 87+. https://doi.org/10.1109/3DUI.2009.4811210.

[39] J.-F. Wu, S.-S. He, F. Wang, Y. Wang, X.-G. Zhao, Q. Wang, Improved resistance matrix approach for readout of the two-dimensional resistive sensor array, Trans. Inst. Meas. Control 41 (2019) 875–882, https://doi.org/10.1177/0142331218774095.

[40] J.-F. Wu, Scanning approaches of 2-D resistive sensor arrays: A review, IEEE Sensors J. 17 (2017) 914–925, https://doi.org/10.1109/JSEN.2016.2641001.

[41] L. Shu, X.M. Tao, D.D. Feng, A wearable, wireless electronic interface for textile sensors lin shu, in: 2010 IEEE International Symposium on Circuits and Systems (ISCAS), 2010, pp. 3104–3107, https://doi.org/10.1109/ISCAS.2010.5537973.

[42] L.Q. Vu, K.H. Kim, L.J.H. Schulze, S.L. Rajulu, Lumbar posture assessment with fabric strain sensors, Comput. Biol. Med. 118 (2020), 103624, https://doi.org/10.1016/j.compbiomed.2020.103624.

[43] F. Pistolesi, B. Lazzerini, Assessing the risk of low back pain and injury via inertial and barometric sensors, IEEE Trans. Ind. Inf. 16 (2020) 7199–7208, https://doi.org/10.1109/TII.2020.2992984.

[44] X. Chen, F. Wang, L. Shu, X. Tao, L. Wei, X. Xu, Q. Zeng, G. Huang, A. Single-material-printed, Low-cost design for a Carbon-based fabric strain sensor, Mater. Des. 221 (2022), 110926, https://doi.org/10.1016/j.matdes.2022.110926.